A Comparative Evaluation of Low-Cycle Fatigue Behavior of Type 316LN Base Metal, 316 Weld Metal, and 316LN/316 Weld Joint

M. VALSAN, D. SUNDARARAMAN, K. BHANU SANKARA RAO, and S.L. MANNAN

A comparative evaluation of the low-cycle fatigue (LCF) behavior of type 316LN base metal, 316 weld metal, and 316LN/316 weld joints was carried out at 773 and 873 K. Total strain-controlled LCF tests were conducted at a constant strain rate of 3×10^{-3} s^{-1} with strain amplitudes in the range ±0.20 to ±1.0 pct. Weld pads with single V and double V configuration were prepared by the shielded metal-arc welding (SMAW) process using 316 electrodes for weld-metal and weld-joint specimens. Optical microscopy, scanning electron microscopy (SEM), and transmission electron microscopy (TEM) of the untested and tested samples were carried out to elucidate the deformation and the fracture behavior. The cyclic stress response of the base metal shows a very rapid hardening to a maximum stress followed by a saturated stress response. Weld metal undergoes a relatively short initial hardening followed by a gradual softening regime. Weld joints exhibit an initial hardening and a subsequent softening regime at all strain amplitudes, except at low strain amplitudes where a saturation regime is noticed. The initial hardening observed in base metal has been attributed to interaction between dislocations and solute atoms/complexes and cyclic saturation to saturation in the number density of slip bands. From TEM, the cyclic softening in weld metal was ascribed to the annihilation of dislocations during LCF. Type 316LN base metal exhibits better fatigue resistance than weld metal at 773 K, whereas the reverse holds true at 873 K. The weld joint shows the lowest life at both temperatures. The better fatigue resistance of weld metal is related to the brittle transformed delta ferrite structure and the high density of dislocations at the interface, which inhibits the growth rate of cracks by deflecting the crack path. The lower fatigue endurance of the weld joint was ascribed to the shortening of the crack initiation phase caused by surface intergranular crack initiation and to the poor crack propagation resistance of the coarse-grained region in the heat-affected zone.

I. INTRODUCTION

THE 18-8 group of austenitic stainless steels, such as AISI type 316, 304, and their modified grades, finds applications as structural material for various components of the liquid-metal-cooled fast breeder reactor (LMFBR). The choice of these alloys is based on their excellent high-temperature tensile, creep, fatigue, and creep-fatigue strengths in combination with good fracture toughness and fabricability. With the current ability to control carbon content, the need for stabilization by either titanium and niobium additions to prevent intergranular corrosion or weld-decay has diminished considerably. The lower carbon content of 0.03 pct maximum in AISI 304L and 316L grades, although providing added resistance to sensitization, results in low usable strength that cannot be increased except by strain hardening. In this scenario, nitrogen-alloyed austenitic stainless steels have emerged as viable alternatives with enhanced high-temperature mechanical properties and lesser susceptibility to sensitization and associated intergranular corrosion.

M. VALSAN, Scientific Officer, Materials Development Division, D. SUNDARARAMAN, Scientific Officer, Metallurgy Division, K. BHANU SANKARA RAO, Head, Mechanical Properties Section, Materials Development Division, and S.L. MANNAN, Head, Materials Development Division, are with Indira Gandhi Centre for Atomic Research, Kalpakkam 603 102, Tamil Nadu, India.

Manuscript submitted February 7, 1994.

The use of this alloy for LMFBR components, however, imposes some stringent requirements on the performance of the parent material as well as its welds. This arises due to cyclic thermal stresses on thick section components as a result of the temperature gradients that occur on heating and cooling during start-ups and shutdowns. Resistance to low-cycle fatigue (LCF), hence, is an important consideration in the design, operation, and safety of LMFBR components operating at high temperatures. As a result, the evaluation of elevated-temperature LCF behavior of 316LN stainless steel has received much attention in recent years.[1-9] The primary objectives of these investigations have been to find out the effects of varying nitrogen contents on the LCF properties, to elucidate the mechanism of nitrogen interstitials and precipitates in LCF deformation, and to establish the composition of nitrogen-alloyed 316L steel that would give better LCF resistance than 316 steel. In these studies, nitrogen addition has been reported to be beneficial, and LCF life has been improved at both ambient temperature and 873 K. This beneficial effect of nitrogen has been found to saturate at approximately 0.12 pct of nitrogen. Further, aging has been found to reduce the fatigue life of alloys having higher nitrogen levels, especially at high strain levels. The LCF behavior of 316LN stainless steel welds has not been investigated. Some studies have been reported on the effect of nitrogen on the tensile properties of 16-8-2 welds[10] and 20Cr-9Ni-3Mo stainless steel weld joints.[11]

In the absence of substantial data, ASME Boiler and Pressure Vessel Code Case N-47[12] imposes a limit on the design strains in the weld regions at one-half the value permitted in the base metal for applications at elevated temperatures where creep effects are significant. The deformation restriction arises primarily from the fact that the weld-deposited austenitic stainless steels are often less ductile than the parent material and that the welds are in the as-welded (as-cast) condition while the base-metal microstructure is optimized by solution-annealing treatments. Furthermore, in austenitic stainless steel welds the delta ferrite introduced to reduce their tendency to hot cracking and microfissuring gets transformed to a hard and brittle phase known as sigma phase when these materials are exposed to elevated temperatures (773 to 1173 K) for extended periods of time.[13] This transformation was shown to lead to low ductility creep ruptures when sufficiently high stresses are applied at elevated temperatures. Earlier, the design rules were based on the wrought materials data. Recently, creep and fatigue reduction factors were introduced in the ASME Boiler and Pressure Vessel Code Case N-47. The allowable number of fatigue cycles is one-half the value permitted for the parent metal while the allowable time duration is determined from stress-to-rupture curves obtained by multiplying the parent material stress-to-rupture values by the weld strength reduction factors. The characterization and better understanding of the LCF behavior of weld-metal and weld-joint specimens, and the transformation behavior of delta ferrite and its effects on cyclic deformation and fracture are required before variations in properties of the base metal and weld metal/weld joints can be treated explicitly and quantitatively. In our laboratory, systematic investigations are currently underway on elevated-temperature tensile, creep, and LCF[14] properties to identify suitable filler metal and basic coated electrodes with optimum nitrogen level for LMFBR components fabricated from type 316LN stainless steel. This investigation deals with the comparative study of LCF lives and cyclic stress response behavior of 316LN base metal, 316 SS weld metal, and 316LN/316 SS weld joints at 773 and 873 K.

II. EXPERIMENTAL PROCEDURE

The base metal chosen for present investigations was a nitrogen-alloyed type 316L stainless steel. The chemical composition in weight percent is provided in Table I. This steel was obtained in the form of 2500 × 1500 × 25 mm plates in the mill-annealed condition. The material was solution-treated at 1373 K for 1 hour and then water-quenched in order to have both carbon and nitrogen in solid solution. Cylindrical samples of 25-mm-gage length and 10-mm-gage diameter are used for LCF testing.

A. *Welding Procedure*

Sections of 600 × 150 × 25 mm cut from the mill-annealed plate were joined along the 600-mm length by the shielded metal-arc welding process (SMAW) using type 316 basic coated electrodes of 4-mm diameter. The welding electrodes were soaked for 1 hour at 473 K before the commencement of welding. During welding, the voltage and current were maintained at approximately 25 V and 150 A, respectively. Weld-metal specimens were taken from the weld pads prepared with a 20 deg included angle, single V-groove joint geometry with a 25-mm root gap and a backing strip (Figure 1(a)). Typically, filling of this joint required 25 weld passes. Weld-joint specimens were machined from the weld pads fabricated with a double-V configuration with an included angle of 70 deg, a root face of 2 mm, and a root gap of 3.15 mm (Figure 1(b)). Approximately 15 passes were used to complete this joint. An interpass temperature of 423 K was maintained during welding of both single-V and double-V weld joints. The weld pads were examined by X-ray radiography for their soundness, followed by delta-ferrite measurement using a commercial magne gage. The ferrite content reported are the statistical averages of at least 50 readings (Table II). The average chemical composition of type 316 SS weld metal is given in Table I. Low-cycle fatigue specimens were machined from the central sections of defect-free single-V and double-V weld pads, as per the layout in Figure 1. The stress axis of the base-metal and weld-joint specimens were parallel to the rolling direction of the base plate.

B. *Low-Cycle Fatigue Testing*

Fully reversed total axial strain-controlled LCF tests were conducted at 298, 773, and 873 K in air on base, weld-metal, and weld-joint specimens using a servo-hydraulic machine equipped with a radiant heating furnace. The temperature of the gage section was controlled within ±2 K. A constant strain rate of 3×10^{-3} s^{-1} was employed for all the tests, which were conducted over strain amplitudes in the range from ±0.2 to ±1.0 pct. A triangular strain-time waveform was used as the input signal and the averaged signal from the linear variable differential transducers, fixed on LCF specimen, was measured and controlled during testing. Stress-strain hysteresis loops were recorded continuously to determine the cyclic-dependent changes in the stress and plastic strain ranges.

C. *Metallography*

The general microstructure of the base metal and weld joints was revealed by etching electrolytically in a solution containing 70 pct HNO_3. The LCF-tested samples

Table I. Chemical Composition in Weight Percent

Alloy	C	Mn	Ni	Cr	Mo	N	S	P
316 LN base metal	0.021	1.75	12.0	17.0	2.4	0.078	0.002	0.023
316 weld metal	0.060	1.42	11.9	18.8	2.0	—	0.01	0.009

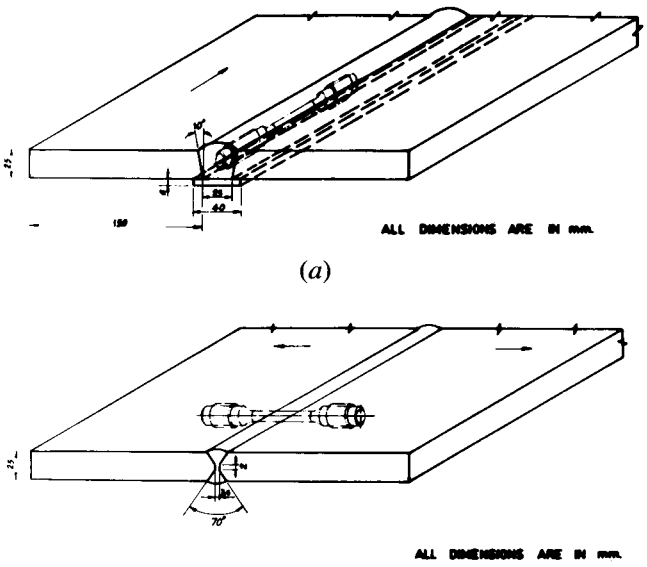

(*a*)

(*b*)

Fig. 1—(*a*) Weld pad geometry for weld-metal samples. (*b*) Weld pad configuration for weld-joint specimens.

were sectioned parallel to the stress loading direction, polished, etched, and examined under optical microscope. The as-welded and LCF-tested weld-metal and weld-joint specimens were etched in modified Murakami's reagent (30 g of KOH, 30 g of $K_3[Fe(CN)_6]$, and 150 mL of water) at 363 K for 15 seconds. Fractography of LCF-tested specimens was carried out by using a PSEM 501 scanning electron microscope. The transmission electron microscopy (TEM) observation was carried out on untested and LCF-tested weld-metal samples using a PHILIPS* EM 400 transmission electron microscope.

*PHILIPS is a trademark of Philips Electronic Instruments Corp., Mahwah, NJ.

III. RESULTS

A. *Cyclic Properties*

The dependence of the peak tensile stress on the number of cycle and on the total strain amplitude for the base, weld-metal, and weld-joint specimens at 773 K is shown in Figures 2, 3, and 4 and at 873 K in Figures 5, 6, and 7, respectively. Cyclic stress response of the weld metal at 298 K is depicted in Figure 8. Base metal generally exhibits very rapid strain hardening to a maximum cyclic stress (Figures 2 and 5). This initial hardening is followed by a regime of nearly stable peak stress. Toward the end of the test, the peak stress amplitude decreases, indicating the formation of macrocracks and their subsequent growth. It is observed that the life spent in the saturation stage is longer as the strain amplitude is lowered. Weld metal undergoes a relatively short period of cyclic hardening in the early stages of fatigue test at all strain amplitudes, followed by a continuous and gradual softening (Figures 3, 6, and 8). However, no saturation stage is observed, unlike the base metal. The rapid load drop toward the end of testing is due to cracking in the specimens. Weld joints also displayed initial hardening followed by gradual softening at all strain amplitudes, except at low strain amplitudes where, in addition, a saturation stage is observed (Figures 4 and 7).

A comparison of the LCF lives of the base-metal, weld-metal, and weld-joint specimens at 773 and 873 K is shown in Figures 9 and 10, respectively. At 773 K, the base metal shows the highest fatigue resistance at most of the strain amplitudes, and the weld joint shows the least fatigue resistance at all strain amplitudes. However, at 873 K, weld metal exhibits an enhanced fatigue strength compared with the base metal.

B. *Microstructural Examination*

1. *Optical and scanning electron microscopy*

The base metal after solutionizing has an average grain size of 85 μm (measured by the linear-intercept

Table II. Magne Gage Readings of Weld-Metal Samples before Fatigue Testing*

	Sample Code Number						
	W12	W13	W14	W15	W16	W17	W18
	Values of x						
	94.5	96.5	95.0	97.5	97.0	96.0	90.5
	94.5	94.0	94.0	97.0	94.5	96.5	93.0
	93.0	90.5	95.5	96.0	93.0	94.0	93.0
	94.0	92.5	100.0	94.0	96.0	95.0	95.0
	94.0	91.0	101.0	93.5	94.5	96.0	96.5
	93.5	96.0	98.0	95.0	91.5	97.5	95.0
	96.5	96.5	97.0	94.0	93.5	94.5	94.0
	96.0	93.0	97.5	92.5	93.0	92.5	94.5
	—	—	99.0	95.0	98.0	92.0	95.0
	—	—	94.0	96.0	96.5	93.5	96.0
	—	—	93.0	—	—	94.0	97.0
Average x	94.5	93.7	96.72	95.0	94.70	94.68	94.5
Average FN	4.86	5.0	4.26	4.72	4.80	4.81	4.86

*Ferrite number (FN) = $(112.5 - x)0.27$.

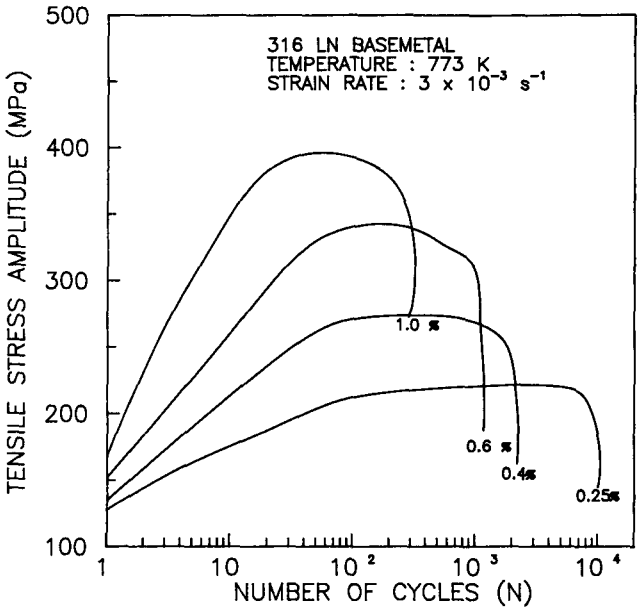

Fig. 2—Cyclic stress response of base metal at 773 K.

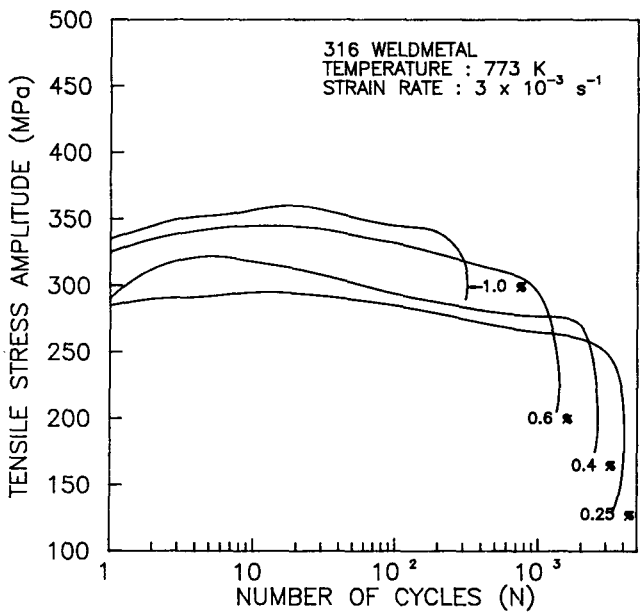

Fig. 3—Cyclic stress response of weld metal at 773 K.

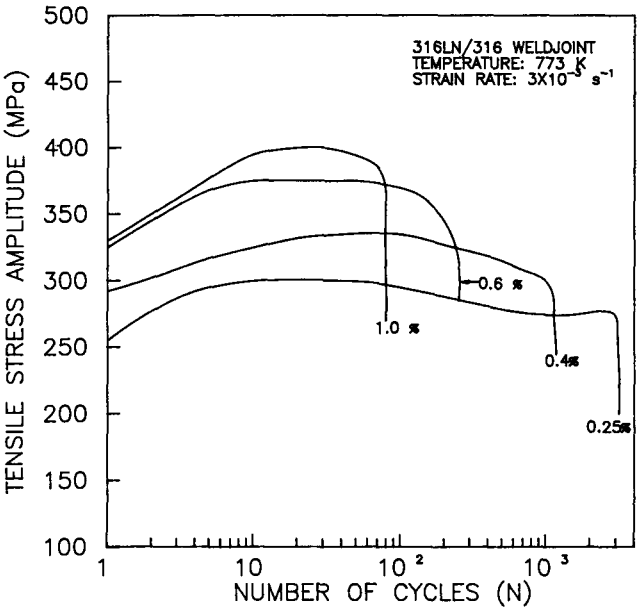

Fig. 4—Cyclic stress response of weld joint at 773 K.

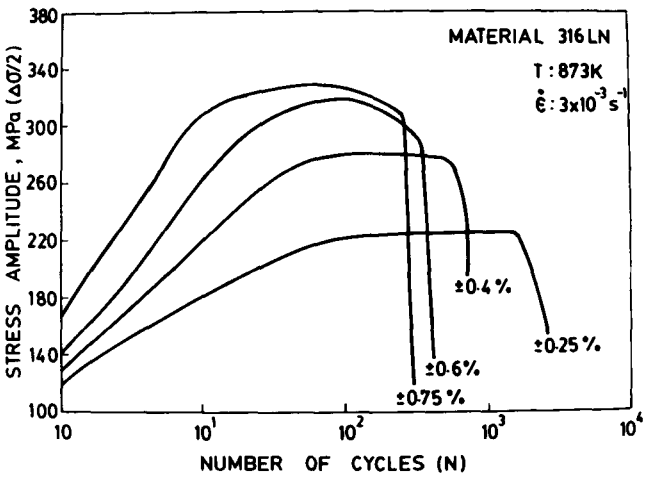

Fig. 5—Cyclic stress response of base metal at 873 K.

method), and the microstructure is free from inclusions and undissolved carbides both in intra- and intergranular regions (Figure 11(a)). The microstructure of the as-deposited 316 SS weld metal, made up of successively overlaid weld beads, is composed of long columnar grains. Delta-ferrite distribution, amount, and morphology differed from pass to pass but remained unchanged within a given pass. The delta-ferrite exhibits a skeletal morphology in the top pass, whereas in a few passes just below the top pass, it has revealed lacy morphology. The vermicular morphology in Figure 11(b) represents the actual delta-ferrite structure in the gage portions of the weld-metal LCF specimens. The average delta-ferrite content in LCF specimens has been estimated as 4.0 to 5.0 ferrite number (FN) by magne-gage measurements. Figure 11(c) shows the representative microstructure in the gage portion of LCF specimens from double-V joint weld joints. The coarse-grained region adjoining the weld metal depicts the heat-affected zone (HAZ), and its width is about 500 μm in size. The average delta-ferrite content of the weld metal in the composite LCF specimens is also 4 to 5 FN. Optical microscopy and scanning electron microscopy (SEM) of fatigue-tested samples reveal that in base metal and weld metal, crack initiation occurs in a purely transgranular mode (Figures 12(a) and (b)). However, in weld joints, crack initiation occurs intergranularly in the HAZ (Figure 12(c)). Fatigue crack propagation is transgranular in base metal at both testing temperatures (Figure 12(a)). Weld joints also exhibit transgranular crack propagation, as evidenced by fatigue striations in Figure 13(a). In weld metal at 873 K, crack path deflection is noticed along the austenite-ferrite interface

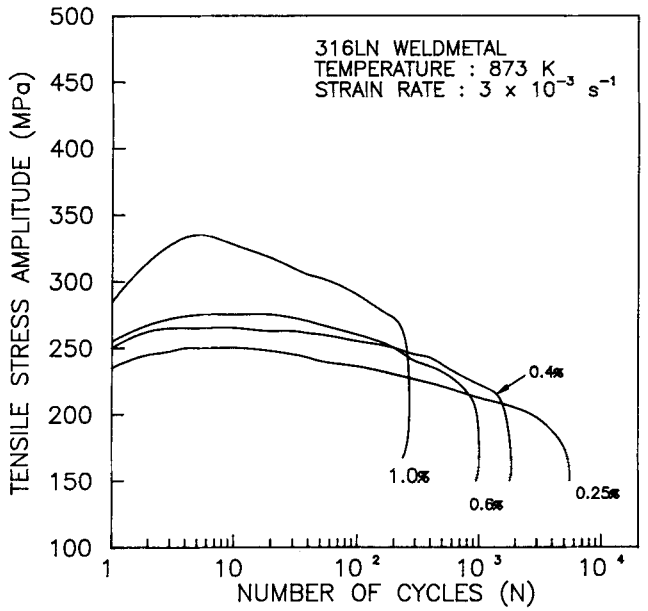

Fig. 6—Cyclic stress response of weld metal at 873 K.

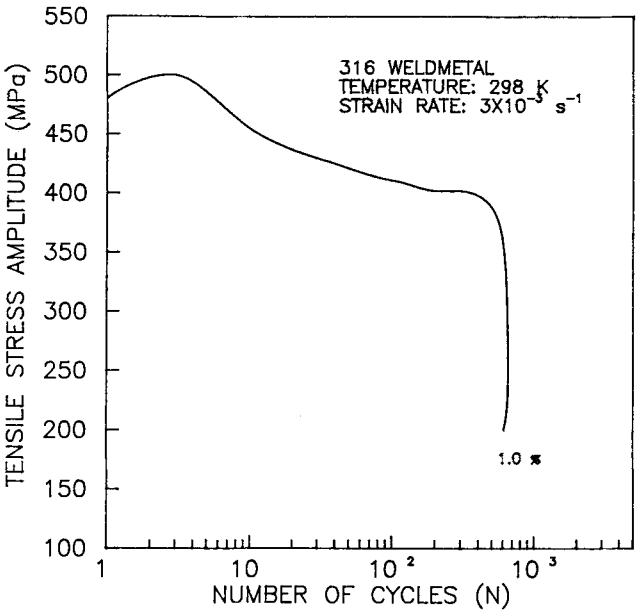

Fig. 8—Cyclic stress response of weld metal at 298 K.

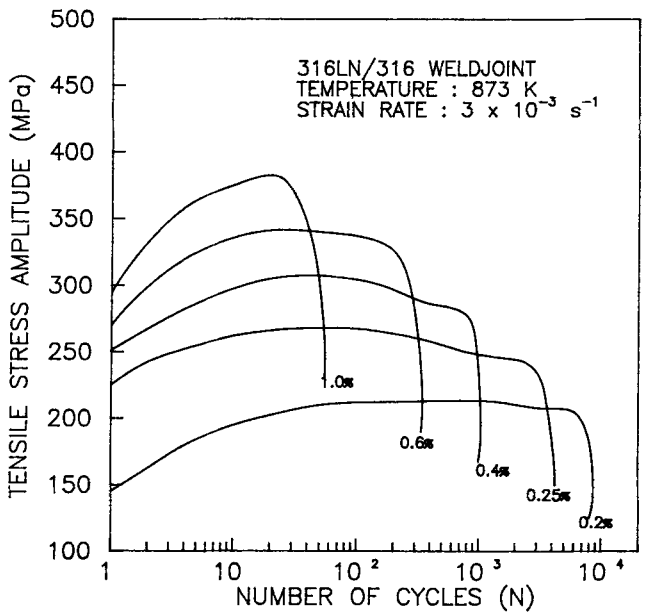

Fig. 7—Cyclic stress response of weld joint at 873 K.

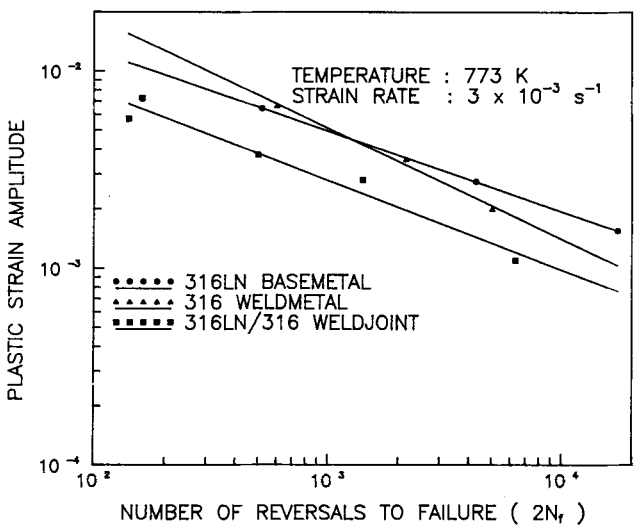

Fig. 9—Comparison of the fatigue lives of base metal, weld metal, and weld joint at 773 K.

(transformed interface) (Figure 13(b)), unlike at 773 K (Figure 13(c)). Furthermore, at 873 K, the number density of secondary cracks on the fracture surface of weld metal is found to be much larger (Figures 14(a) through (c)) compared with 773 K (Figures 14(d) through (f)). The fractographs (Figure 14) represent different regions of the fracture surface and are taken at various magnifications to obtain an overall idea about the extent of secondary cracks.

2. *Transmission electron microscopy*

Transmission electron microscopy of AISI 316 weld metal has been carried out on untested samples and on samples tested at strain amplitudes of ±0.25 to ±1.0 pct at 873 K. Untested samples revealed very high dislocation density and extensive precipitation of carbides (Figure 15). Dislocation structure is mainly tangles distributed in the austenite matrix. In the untested condition, delta ferrite also contained dislocations, though the density is much lower compared with the corresponding untested austenite matrix. Figure 15(a) represents high dislocation density in the austenite matrix and isolated dislocations in the delta ferrite, and Figure 15(c) depicts high dislocation density in the untested austenite matrix away from the interface. Occasionally, as-welded matrix is found to be highly twinned with the twin bands extending up to the delta-ferrite boundaries (Figure 15(d)). Carbides are found in the delta-ferrite-austenite boundaries (Figures 15(a) and (b)), in the austenite matrix (Figures 15(a) and (c)), and also in the twin bands (Figure 15(e)). Selected area diffraction (SAD) of carbides in Figure 15(a) is depicted in Figure 15(f), and the

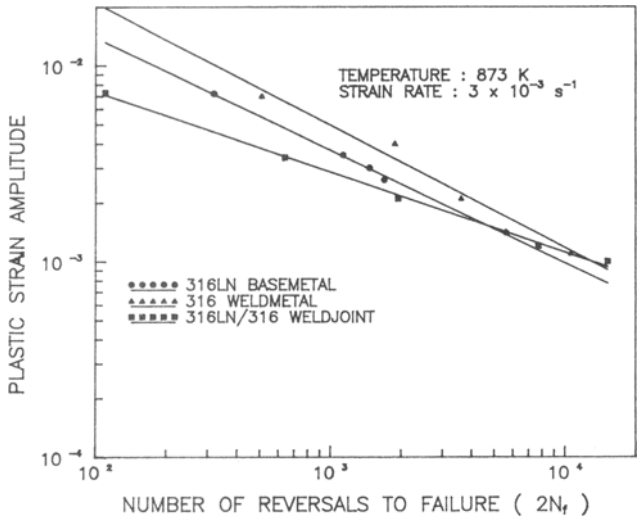

Fig. 10—Comparison of the fatigue lives of base metal, weld metal, and weld joint at 873 K.

key to it is in Figure 15(g). Diffraction spots from delta ferrite is also shown in Figure 15(f). After testing at low strain amplitudes (±0.25 pct), the dislocation density is seen to be much lower at regions away from the delta-ferrite-austenite boundary (Figure 16(a)) compared with the untested samples (Figure 15(c)). Furthermore, the delta ferrite is completely free of dislocations, and the $M_{23}C_6$ carbides have coarsened considerably (Figure 16(b)). Figure 16(c) (strain amplitude = ±1.0 pct) shows nearly dislocation-free delta ferrite surrounded by a thick boundary consisting of a high density of dislocation tangles. Farther away from this boundary austenite matrix exhibits dislocation structure, typically as shown in Figure 16(a). Selected area diffraction of delta ferrite in Figure 16(c) is provided in Figure 16(d), and the key to it is in Figure 16(e). Figure 17 shows the delta ferrite and austenite matrix of samples fatigue tested at strain amplitudes of ±0.4 pct. The dislocation density near the interface is found to increase with strain amplitude.

IV. DISCUSSION

A. *Cyclic Stress Response*

The substantial initial hardening followed by stress saturation seen in base metal (Figures 2 and 5) was also noted previously by several others[1,2] in the nitrogen-alloyed type 316L steels at 873 K. Further, this type of cyclic stress response has been pointed out to be a characteristic phenomenon of homogeneous solid solutions and is reported to occur when nitrogen content is less than 0.1 wt pct.[11] However, when the dissolved nitrogen content is high, the alloy shows a softening regime after the initial hardening (in room-temperature fatigue tests), and when the samples with high nitrogen content are aged for long times, the material fails after the initial hardening without a saturation regime.[3] The considerable hardening in the initial stages can result from individual or combined effects of (1) mutual interaction among dislocations, (2) formation of fine precipitates on

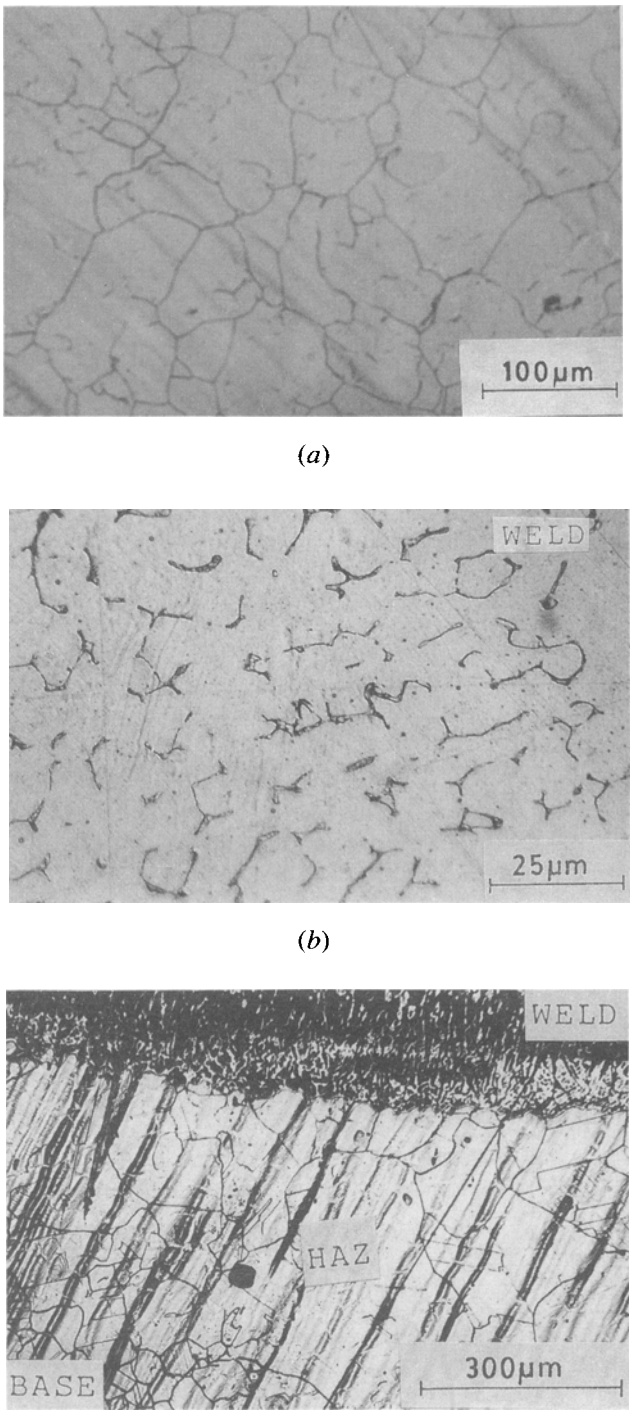

Fig. 11—Prior microstructures of (*a*) base metal, (*b*) weld metal, and (*c*) weld joint.

dislocations during testing, and (3) interaction between dislocations and solute atoms.

It must be pointed out that the duration of the LCF tests is short so that no precipitation of carbides on dislocations during strain cycling is expected. Also, the addition of nitrogen is reported to delay the precipitation of carbides in the static aging condition.[15] Furthermore, the rapid cyclic hardening is also reported in the tests performed in the range 723 to 823 K,[14] where the test

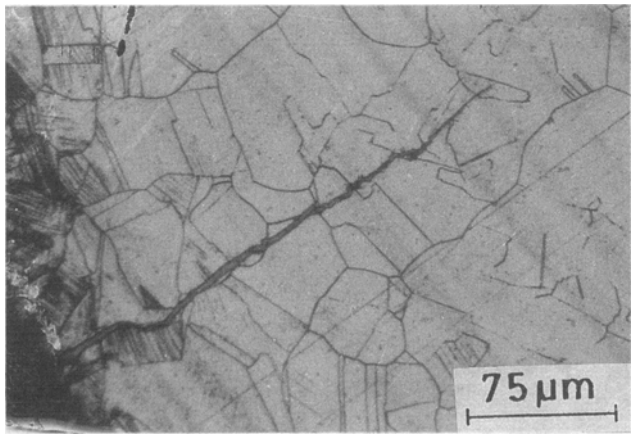

(*a*)

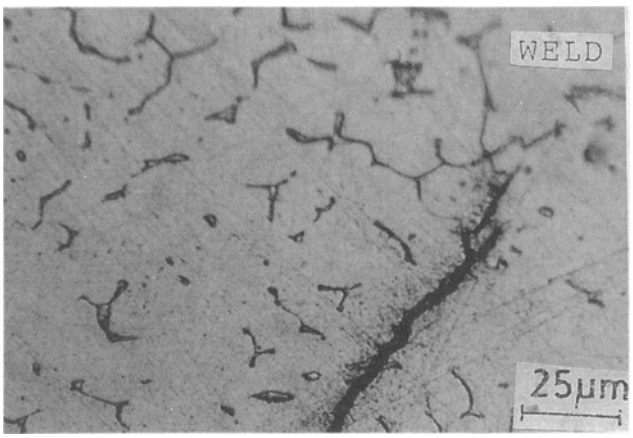

(*b*)

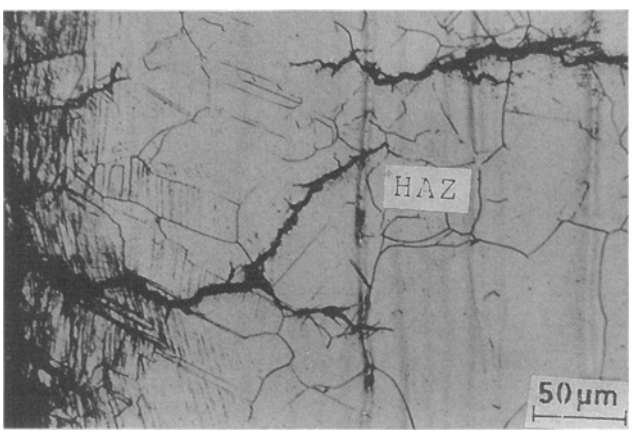

(*c*)

Fig. 12—(*a*) Transgranular crack initiation in base metal (±0.4 pct, 873 K). (*b*) Transgranular crack initiation in weld metal (±0.25 pct, 873 K). (*c*) Intergranular crack initiation in weld joint (±0.25 pct, 873 K).

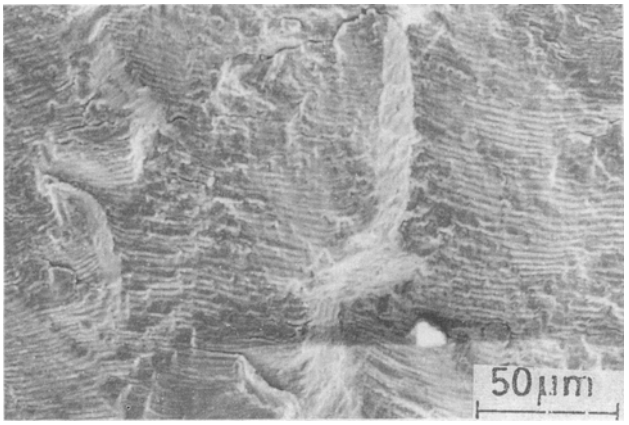

(*a*)

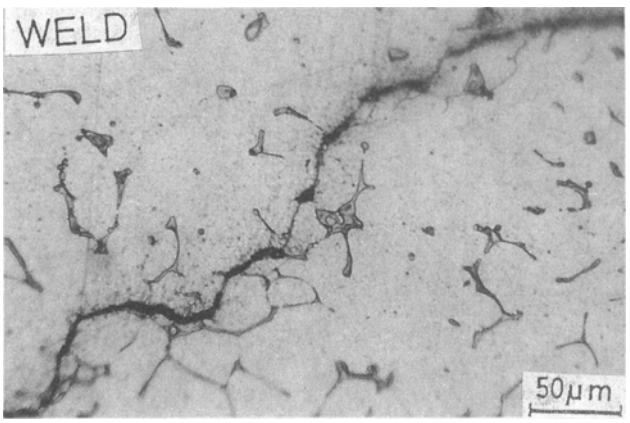

(*b*)

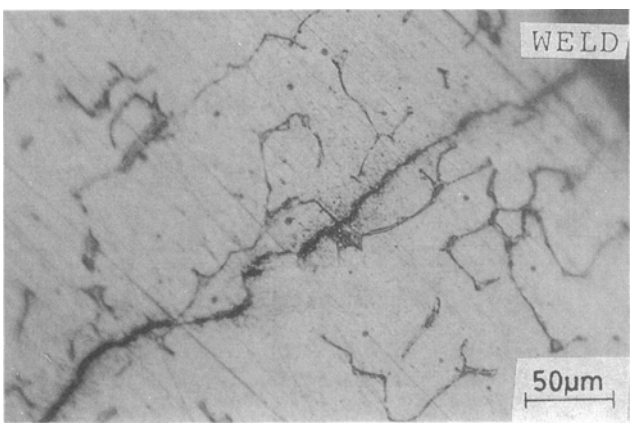

(*c*)

Fig. 13—(*a*) Striations on HAZ regions in weld joints (873 K, ±0.25 pct). (*b*) Crack deflection in weld metal along transformed grain boundaries (873 K). (*c*) Reduced crack path deflection in weld metal (773 K).

temperatures are too low to cause dynamic precipitation. In addition, it was reported that for 316LN steel of similar composition, static aging causes a decrease in the hardening with an increase in aging time.[3] These observations clearly rule out the role of carbide precipitates in causing the rapid hardening.

Intense cyclic hardening marked by serrated flow during LCF was observed by Degallaix *et al.* in nitrogen-alloyed 316L steels.[3] This results from the high mobility of interstitial atoms leading to the formation of Cottrell atmospheres around dislocations. The TEM evidence for pinning by solute atmospheres in this

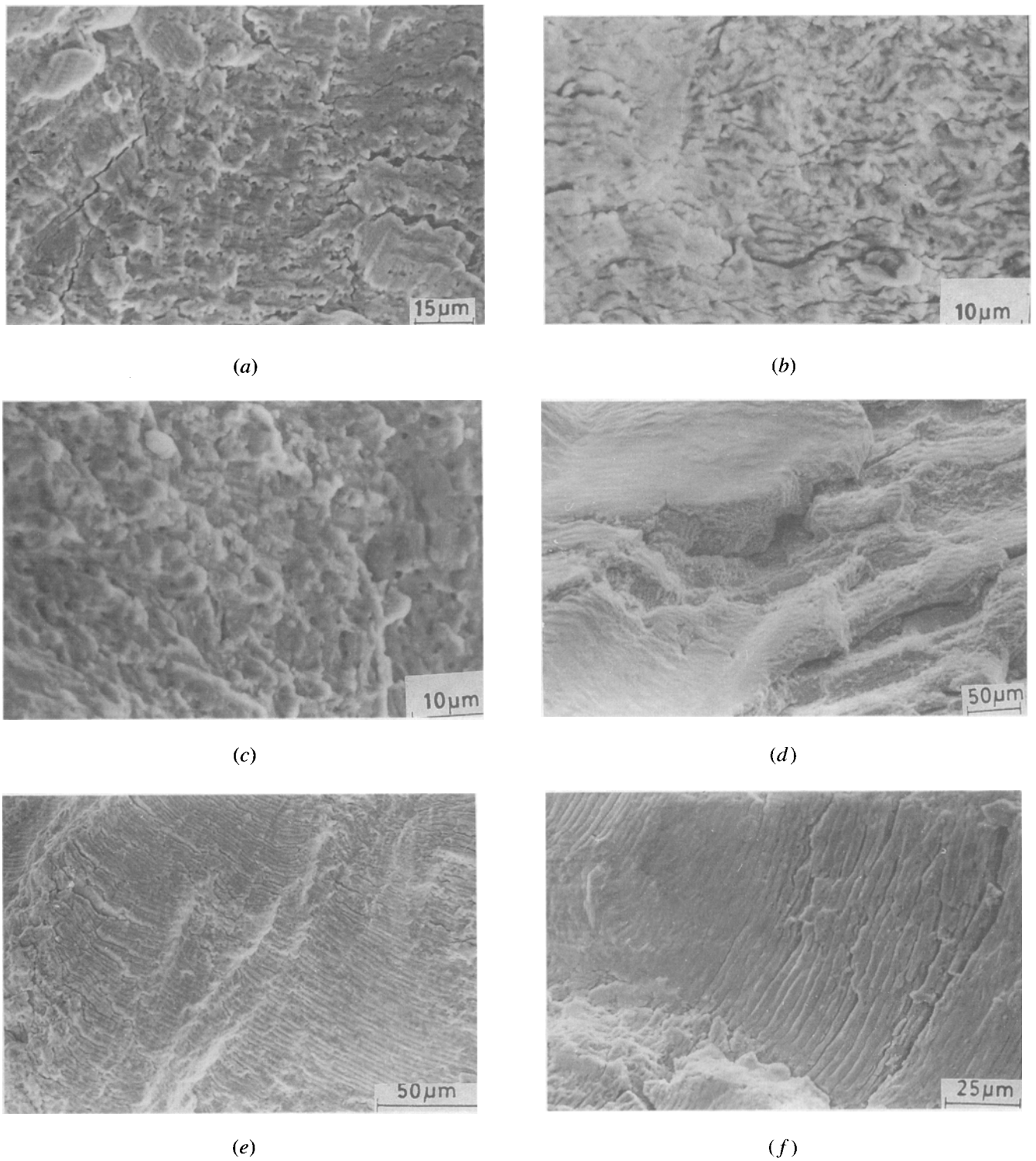

Fig. 14—(*a*) through (*c*) Large number density of secondary cracks in weld metal at 873 K, ±0.25 pct. (*d*) through (*f*) Less number density of secondary cracks in weld metal at 773 K, ±0.25 pct.

steel was provided by Srinivasan *et al.*[114] Though serrated flow could not be observed in this investigation at 873 K at a strain rate of 3×10^{-3} s^{-1}, the LCF tests conducted in the range 573 to 873 K showed an increase in the peak tensile stress with an increase in temperature, exhibiting a maximum at 873 K.[114] The negative temperature dependence of peak tensile stress was established as one of the manifestations of dynamic strain aging (DSA) in LCF.[116,17] Further, there was a recent study[118] on the thermal aging effects in 316LN in the temperature range 873 to 1173 K for various durations. The study illustrates the formation of Cr_2N ordered zones on aging at 873 K for 25 hours, unambiguously. The formation of the Cr_2N phase is associated with the production of $a/2$ ⟨110⟩ dislocation pairs in the gamma matrix. It is suggested[119] that at shorter aging times,

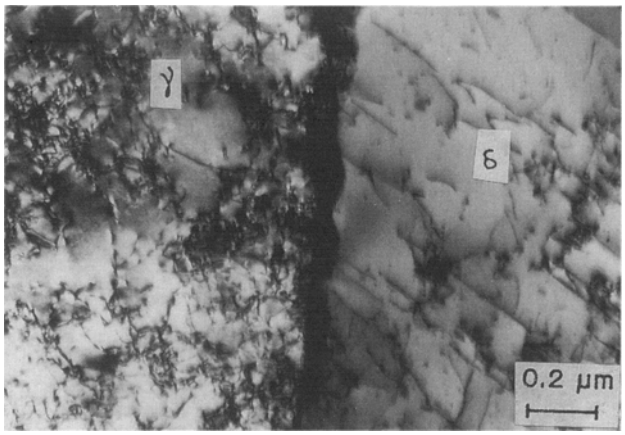

(*a*)

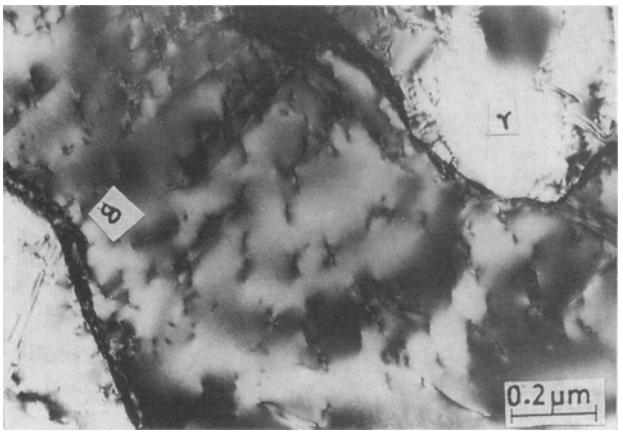

(*b*)

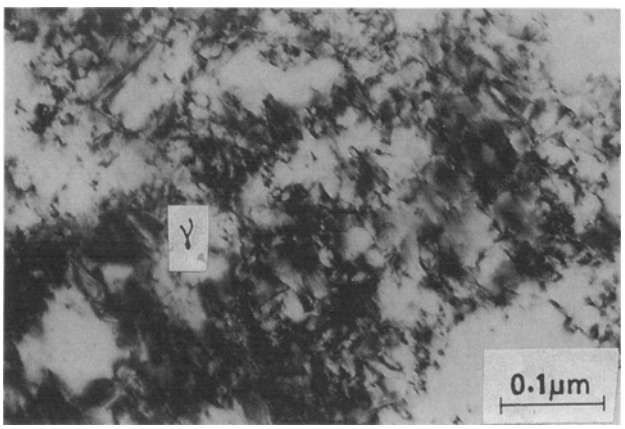

(*c*)

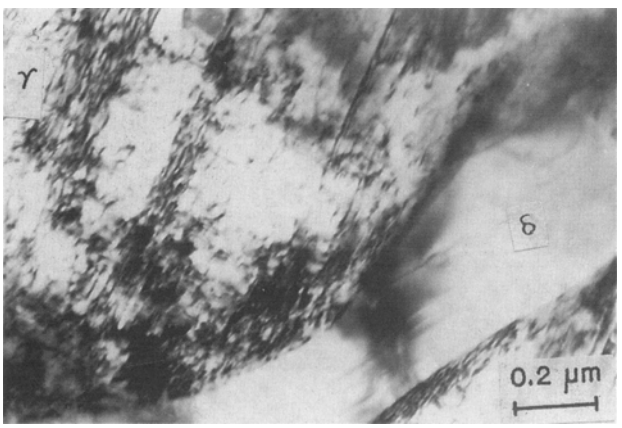

(*d*)

Fig. 15—(*a*) High dislocation density in untested austenite matrix and isolated dislocations in delta-ferrite. (*b*) Another region of untested delta-ferrite. (*c*) Dislocation tangles in untested austenite matrix away from the boundary. (*d*) Twin bands in untested austenite matrix. (*e*) Precipitation in twin bands. (*f*) SAD of the carbides and delta ferrite in (a). (*g*) Key to SAD.

substitutional-interstitial complexes of a few atom layers thick can also lead to rapid initial strain hardening due to the increased resistance of dislocation motion in the ordered domains in the matrix. Thus, the initial hardening observed in base-metal 316LN can be attributed to the combined effects of dislocation-solute atom/complexes interaction and dislocation-dislocation interaction.

The stress-saturation stage following the initial hardening in low nitrogen 316L stainless steel has been reported to be associated with the development of dislocation cells.[3] However, in this steel, only moderate tendency was reported for cell formation at these testing temperatures.[14] The basis for the occurrence of stress saturation consequent to the development of cells is attributed to the cell-shuttling motion of dislocations. However, in the absence of cells, stress saturation can be conceived when the number density of slip bands gets saturated and the mean free path of mobile dislocations is restricted to the inter–slip band spacing.[20] It is assumed that the slip band intersections have a complex configuration, and they act as impenetrable obstacles to the motion of dislocations.[20]

Weld metal displayed a gradual softening regime for the major portion of the life after an initial short period of hardening (Figures 3, 6, and 8). Similar stress response behavior was reported earlier in the case of type 16Cr-8Ni-2Mo weld metal at 866 K[8] and in 308 weld metal in the temperature range 823 to 923 K.[21] In these steels, the cyclic softening is thought to occur either due to the annihilation of dislocations or due to the rearrangement of dislocations to cells/subgrains.

In order to elucidate the operative deformation mechanism in this investigation, detailed TEM of 316 weld metal was carried out on untested samples and on samples tested at strain amplitudes of ±0.25 to ±1.0 pct and at temperatures of 773 and 873 K. Untested samples reveal a very high dislocation density and precipitation of carbides (Figure 15). Dislocation structure is mainly tangles distributed in the austenite matrix. In the untested condition, delta ferrite also contained some amount of dislocations.

The configuration of dislocations in the austenite matrix of the weld metal in the untested samples resembles that of a highly cold-worked structure, and it has been reported by Reddy *et al.*[22] that type 316 SS weld

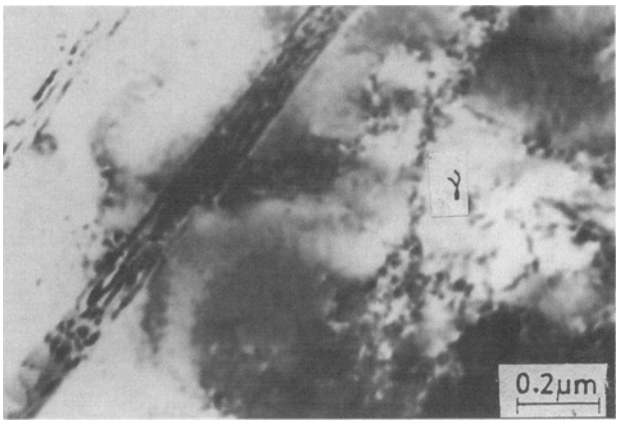

(*e*)

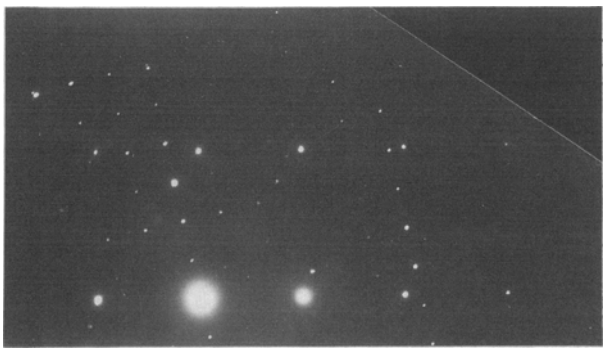

(*f*)

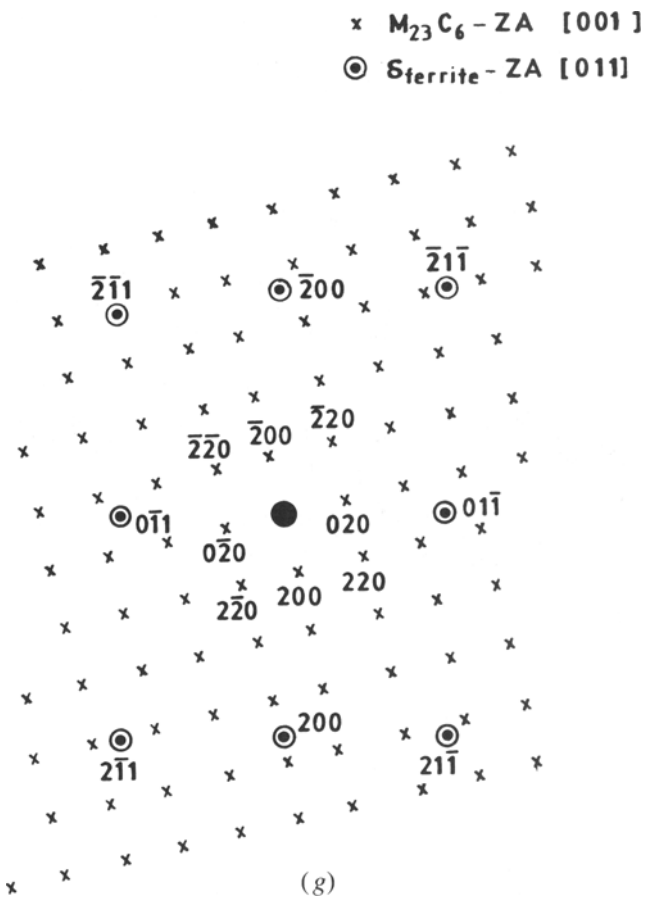

(*g*)

Fig. 15 Cont.—(*a*) High dislocation density in untested austenite matrix and isolated dislocations in delta-ferrite. (*b*) Another region of untested delta-ferrite. (*c*) Dislocation tangles in untested austenite matrix away from the boundary. (*d*) Twin bands in untested austenite matrix. (*e*) Precipitation in twin bands. (*f*) SAD of the carbides and delta ferrite in (a). (*g*) Key to SAD.

metal contains high dislocation densities of the order of $8 \times 10^9/cm^2$. This high dislocation density results from shrinkage stresses present during cooling of the weld metal during welding operations. The severity of the shrinkage stresses is also reflected in certain areas where deformation occurs by twinning (Figures 15(d) and (e)), which is energetically a less favorable deformation process compared to glide. It is also noticed that deformation is not carried through the austenite-ferrite boundary, and delta ferrite is generally deformed to a less extent (Figure 15). This can be attributed to the differences in the flow stresses of the two phases. This observation is consistent with that reported in 308 stainless steel weld metal in which there is a difference in the nanohardness of the ferrite and the austenite phases, and the former is observed to be harder even in unaged conditions.[23]

In the absence of any cells or subgrains after fatigue testing, the possibility that the dislocations in the untested condition (dislocation tangles, Figure 15(c)) getting rearranged into these low-energy configurations is unlikely. Since the final dislocation density in both the austenite (at regions far away from the boundary) and ferrite phases are much lower, the mechanism of dislocation annihilation leading to cyclic softening can be operative. It is conceived that during repeated cyclic loading, dislocation tangles break down, and subsequently, annihilation of dislocations of the opposite sign occurs during their to and fro motion. Further, since austenite delta-ferrite interphase boundaries can act as

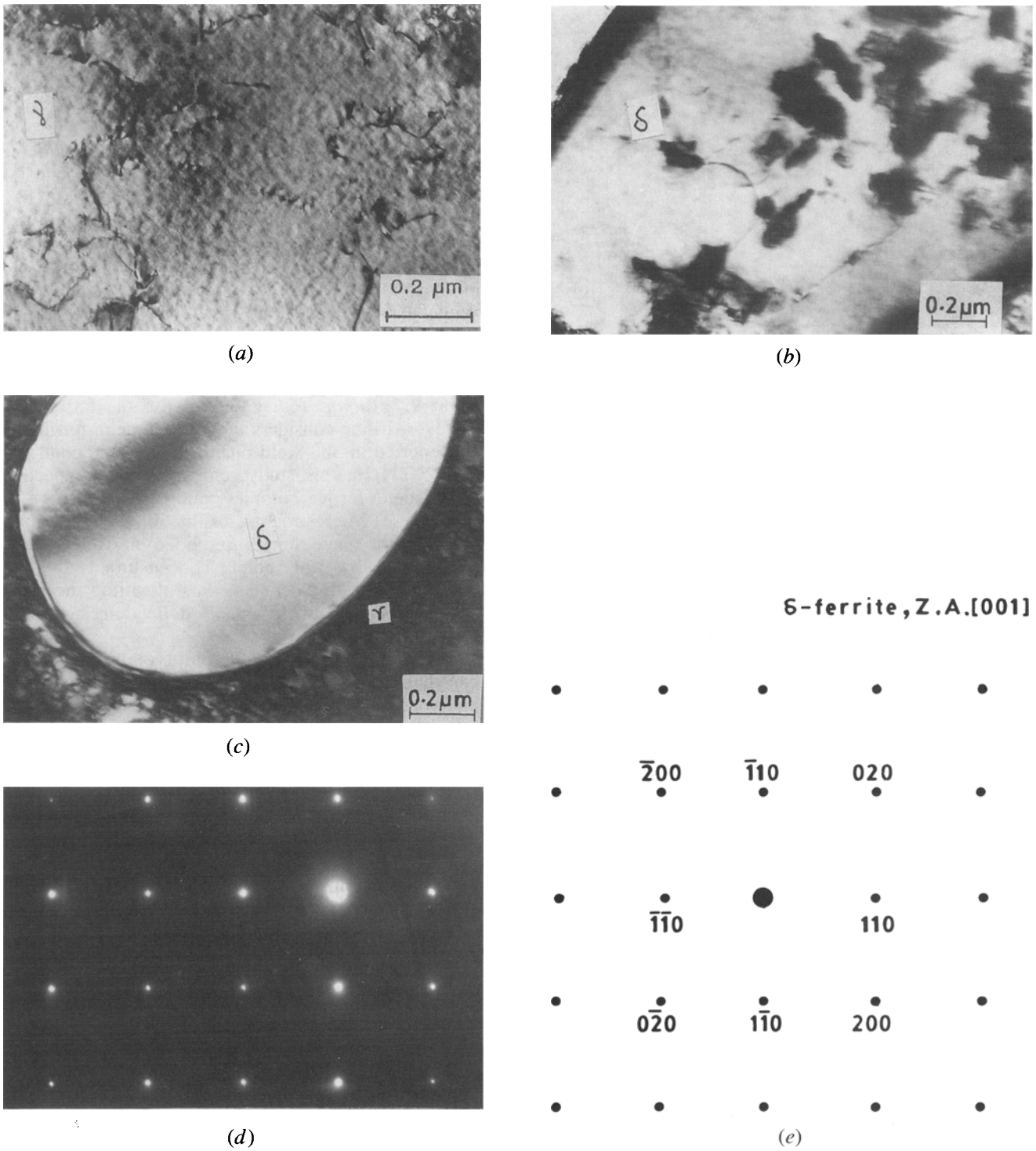

Fig. 16—(*a*) Low dislocation density in austenite matrix after testing at ±0.25 pct, 873 K. (*b*) Low dislocation density and coarse carbides at ±0.25 pct, 873 K. (*c*) Low dislocation density in delta ferrite after testing at ±1.0 pct, 873 K. (*d*) Delta-ferrite SAD in (c). (*e*) Key to SAD.

sinks, dislocations get annihilated at the interphases as well. However, the interface regions can also act as sources of dislocations, and consequently, these regions have a generally high dislocation density, which is in accordance with the applied strain amplitude. In such situations, high strain fatigue is caused by dislocations near the austenite delta-ferrite interphase boundaries.

The cyclic stress response of weld joints is marked by initial cyclic hardening (Figures 4 and 7) similar to the base metal (Figures 2 and 5), although the degree hardening is less. This behavior can be justified since the major part of the gage length is made up of the base metal, and consequently, the initial cyclic deformation of the weld joint will be similar to that of its major

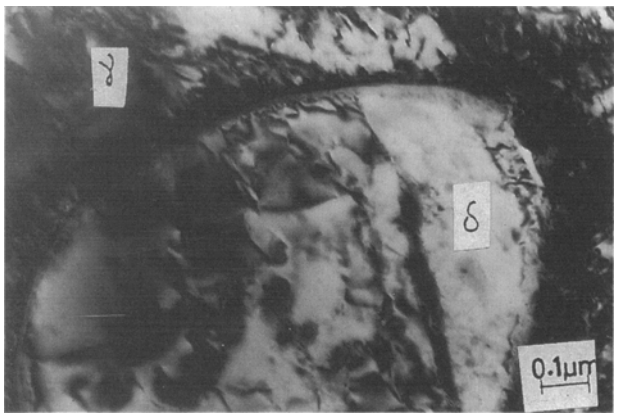

Fig. 17—TEM micrograph representing low dislocation density and coarse carbides in delta ferrite and dislocation tangles near boundary at ±0.4 pct, 873 K.

constituent. Furthermore, the occurrence of saturation at the lower strain amplitudes in the weld joint (Figures 4 and 7) like in the base metal (Figures 2 and 5) suggests the predominance of deformation in the base metal or the microstructurally altered region, *i.e.*, the HAZ.

C. *Fatigue Life and Fracture Behavior*

The LCF life is generally governed by the tensile ductility of the material. Therefore, one will expect lower fatigue life for weld metal (a cast structure), which is less ductile than base metal. Contrary to this, weld metal showed a better fatigue life than the base metal at 873 K (Figure 10). This can result from the crack propagation differences between the base and weld metals. The fine duplex austenite-ferrite microstructure in the weld metal, with its many transformed phase boundaries, offers a greater resistance to the extension of fatigue cracks by causing deflection of the crack path (Figure 13(b)) than does the coarser structure of the base metal (Figure 12(a)). Furthermore, the increased resistance to crack propagation can also be attributed to the presence of heavily dislocated interphase boundaries between the austenite and delta phase (Figures 16(c) and 17). A tangled dislocation structure near the phase boundary coupled with the brittle transformed interface leads to cracking of the latter, resulting in a deflection of the crack path. Crack deflection leads to reduced stress intensity at the crack tip and an associated reduction in the crack propagation rate. However, it must be pointed out that a highly dislocated region near the interface alone (without a brittle transformed region) is not sufficient to affect the crack path deflection. This is evident in tests conducted at 773 K.

At 773 K, fatigue resistance of weld metal is lower at all strain amplitudes compared with the base metal (Figure 9). This could be associated with the reduced degree of transformation of delta ferrite to the brittle sigma phase and carbides at 773 K and the associated decrease in the degree of crack path deflection (Figure 13(c)). The percent of delta ferrite transformed during testing was determined by magne-gage measurements. Table III clearly indicates the extent of transformation at 873 K compared with 773 K. Furthermore, microcracking is more pronounced in samples tested at 873 K compared with samples tested at 773 K. This is associated with the transformation of delta ferrite to the brittle sigma phase at 873 K. An enhanced degree of secondary cracks on the fracture surface marked by fatigue striations is shown in Figures 14(a) through (c) for samples tested at 873 K. However, secondary cracking is relatively less at 773 K (Figures 14(d) through (f)). These fractographs taken at different magnifications at various places on the fracture surface provide an overall information regarding the extent of secondary cracks in weld metal at two test temperatures. From these, it is inferred that at 773 K, weld metal shows a lower life compared with base metal (Figure 9).

It must be pointed out that, contrary to the present observation, in an earlier work on 308 weld metal[21] microcracking of brittle sigma phase during fatigue testing at 923 K was found to decrease the fatigue life. However, if one considers the average delta-ferrite content reported in 308 weld metal (9 FN)[21] in contrast to (4 to 5 FN) in this study, enhanced interconnectivity among delta-ferrite colonies can be expected in the former case. Microstructure of the 308 weld metal representing the gage length provided in Reference 21 clearly brings out this point. This in turn leads to the linkup of these microcracks, thus offsetting the advantages associated with crack deflection and crack branching.

The fatigue life of the weld joint is significantly lower than that of the weld metal and the base metal at both the temperatures investigated. This decrease in life corresponds to a transition in crack initiation mode from purely transgranular in base (Figure 12(a)) and weld metals (Figure 12(b)) to an intergranular one in the HAZ of the weld joint (Figure 12(c)). This intergranular crack initiation results as a consequence of the planar slip band impingement on the grain boundaries. Movement of dislocations in planar slip bands leads to the formation of dislocation pileups at the intersection of grain boundary and slip bands. The stress concentration arising out of such pileups has been suggested to cause intergranular cracking more easily in coarse-grained stainless steel.[24] Surface intergranular cracking shortens the crack initiation phase in weld joints and reduces the overall fatigue life. In alloys deforming by planar slip, an improved crack propagation resistance can be conceived with decreasing grain size; the grain boundaries serve as barriers to transgranular crack propagation, causing the crack front to be held back and necessitating a crack initiation event to occur in each new grain. Since, in the weld joints, crack propagation is transgranular in the HAZ

Table III. Percentage of Delta Ferrite Transformed after Fatigue Testing

	Strain Amplitude (Pct)			
	±0.25	±0.4	±0.6	±1.0
Temperature	Percentage of Delta Ferrite Transformed			
873 K	16	25	40	40
773 K	2	—	—	—

containing coarse grain size, it can be argued that the crack propagation resistance in weld joints is also reduced.

V. CONCLUSIONS

1. The cyclic stress response of the base metal is characterized by initial hardening followed by a well-defined saturation stage, whereas in weld metal, a brief period of initial hardening is followed by an extended gradual softening stage. Weld joints initially hardened like base metal and then softened gradually like weld metal. At low strain amplitudes, the softening stage of weld joints ends in a stress plateau, which continues up to fracture.
2. Initial hardening in the base metal has been mainly attributed to the interaction between dislocations and solute atoms/complexes and cyclic saturation to saturation in the number density of slip bands. From TEM studies, the cyclic softening in weld metal has been ascribed to the annihilation of dislocations during repeated cyclic loading conditions.
3. Type 316LN base metal exhibits better fatigue resistance than weld metal at 773 K, whereas the reverse holds true at 873 K. At both temperatures, weld joints have the lowest fatigue life.
4. The better fatigue resistance of weld metal at 873 K has been attributed to the brittle transformed delta-ferrite structure and high density of dislocation tangles at the interface that inhibits the growth rate of cracks by deflecting the crack path. At 773 K, crack path deflection is minimum, and weld metal shows lower life than base metal.
5. The poor fatigue resistance of the weld joint has been ascribed to the shortening of the crack initiation phase, resulting from surface intergranular crack initiation and poor crack propagation resistance of the coarse-grained region in the HAZ. Surface intergranular crack initiation in the HAZ resulted from the impingement of planar slip bands on the grain boundary.

ACKNOWLEDGMENT

The authors wish to thank Dr. Placid Rodriguez, Director, IGCAR, for his encouragement and many useful discussions in the course of this investigation.

REFERENCES

1. R. Taillard, S. Degallaix, and J. Foct: *Low Cycle Fatigue and Elasto Plastic Behaviour of Materials*, K.T. Rie, ed., Elsevier, Munich, 1987, pp. 83-88.
2. R. Sandstrom, J. Engstrom, J.O. Nilsson, and A. Nordgren: *High Temp. Technol.*, 1989, vol. 7, pp. 2-9.
3. S. Degallaix, G. Degallaix, and J. Foct: *Low Cycle Fatigue*, ASTM STP 942, 1988, pp. 798-811.
4. J.O. Nilsson: *Fatigue Eng. Mater. Struct.*, 1984, vol. 7 (1), pp. 55-64.
5. B. Vogt, S. Degallaix, and J. Foct: *Int. J. Fatigue*, 1984, vol. 6 (4), pp. 211-15.
6. J.O. Nilsson: *Scripta Metall.*, 1983, vol. 17, pp. 593-96.
7. R. Taillard and J. Foct: in *Proc. Int. Conf. on High Nitrogen Steels 88*, J. Foct and A. Hendry, eds., The Institute of Metals and the Societe Francaise de Metallurgie, Lille, France, 1988, May, pp. 387-91.
8. S. Degallaix: Ph.D. Thesis, Universite des Sciences et Techniques de Lille, Lille, France, 1986.
9. J.O. Nilsson and T. Thorvaldsson: *Scand. J. Metall.*, 1985, vol. 15, pp. 83-89.
10. K. Borst and M. Pohl: in *Proc. Int. Conf. on High Nitrogen Steels 88*, J. Foct and A. Hendry, eds., The Institute of Metals and the Societe Francaise de Metallurgie, Lille, France, 1988, May, pp. 294-99.
11. G.A. Honeyman and T.A. Towers: in *Proc. Int. Conf. on High Nitrogen Steels 88*, J. Foct and A. Hendry, eds., The Institute of Metals and the Societe Francaise de Metallurgie, Lille, France, 1988, May, pp. 398-404.
12. ASME Boiler and Pressure Vessel Code Case N-47, ASME, New York, NY, 1986.
13. M.O. Malone: *Weld. J.*, 1967, vol. 46, p. 241S.
14. V.S. Srinivasan, R. Sandhya, K. Bhanu Sankara Rao, S.L. Mannan, and K.S. Raghavan: *Int. J. Fatigue*, 1991, vol. 13 (6), pp. 471-78.
15. Erich Folkhard: *Welding Metallurgy of Stainless Steels*, Springer-Verlag/Wien, New York, NY, 1988, p. 103.
16. K. Bhanu Sankara Rao, M. Valsan, R. Sandhya, S.L. Mannan, and P. Rodriguez: *Met. Mater. Process.*, 1990, vol. 2, pp. 17-36.
17. M. Valsan, D.H. Sastry, K. Bhanu Sankara Rao, and S.L. Mannan: *Metall. Mater. Trans. A*, 1994, vol. 25A, pp. 159-71.
18. P. Shankar, D. Sundararaman, and S. Ranganathan: *Scripta Metall. Mater.*, 1994, vol. 31 (5), pp. 589-93.
19. D. Sundararaman, P. Shankar, and V.S. Raghunathan: *Metall. Mater. Trans. A*, in press.
20. M. Valsan: Ph.D. Thesis, Indian Institute of Science, Bangalore, 1991.
21. K. Bhanu, Sankara Rao, M. Valsan, and S.L. Mannan: *Mater. Sci. Eng.*, 1990, vol. A130, pp. 67-82.
22. A.S. Reddy, S.L. Mannan, V. Seetharaman, and P. Rodriguez: *Proc. National Welding Seminar*, New Delhi, 1980, paper 21.
23. J.M. Vitek, S.A. David, D.J. Alexlander, J.R. Keiser, and R.K. Nanstad: *Acta Metall.*, 1991, vol. 39 (4), pp. 503-16.
24. K. Bhanu Sankara Rao, M. Valsan, R. Sandhya, S.L. Mannan, and P. Rodriguez: *High Temp. Mater. Process.*, 1986, vol. 7, pp. 171-77.